Franck-Condon simulation of vibrationally resolved optical spectra for zinc complexes of phthalocyanine and tetrabenzoporphyrin including the Duschinsky and Herzberg-Teller effects

Meiyuan Guo, Rongxing He, Yulan Dai, Wei Shen, Ming Li, Chaoyuan Zhu, and Sheng Hsien Lin

Citation: The Journal of Chemical Physics **136**, 144313 (2012); doi: 10.1063/1.3703310
View online: http://dx.doi.org/10.1063/1.3703310
View Table of Contents: http://scitation.aip.org/content/aip/journal/jcp/136/14?ver=pdfcov
Published by the AIP Publishing

Franck-Condon simulation of vibrationally resolved optical spectra for zinc complexes of phthalocyanine and tetrabenzoporphyrin including the Duschinsky and Herzberg-Teller effects

Meiyuan Guo,[1] Rongxing He,[1,a)] Yulan Dai,[1] Wei Shen,[1] Ming Li,[1] Chaoyuan Zhu,[2,b)] and Sheng Hsien Lin[2]
[1]*College of Chemistry and Chemical Engineering, Southwest University, Chongqing 400715, China*
[2]*Department of Applied Chemistry, Institute of Molecular Science and Center for Interdisciplinary Molecular Science, National Chiao-Tung University, Hsinchu 300, Taiwan*

(Received 9 January 2012; accepted 28 March 2012; published online 13 April 2012)

High resolved absorption and fluorescence spectra of zinc complexes of phthalocyanine (ZnPc) and tetrabenzoporphyrin (ZnTBP) in the region of Q states were reported. Few theoretical investigations were performed to simulate the well-resolved spectra and assigned the vibrational bands of the large molecules, especially for high symmetrical characteristic molecules, on account of the difficulties to optimize the excited states and analyze a large number of final vibrational-normal modes. In the present work, the $S_0 \leftrightarrow S_1$ absorption and fluorescence spectra (that is, the Q band) of ZnPc and ZnTBP were simulated using time-dependent density functional theory with the inclusions of Duschinsky and Herzberg-Teller contributions to the electronic transition dipole moments. The theoretical results provide a good description of the optical spectra and are proved to be in excellent agreement with experimental spectra in inert-gas matrices or in supersonic expansion. This study focused attentions on the optical spectral similarities and contrasts between ZnPc and ZnTBP, in particular the noticeable Duschinsky and Herzberg-Teller effects on the high-resolved absorption and fluorescence spectra were considered. Substitution of *meso*-tetraaza on the porphyrin macrocycle framework could affect the ground state geometry and alter the electron density distributions, the orbital energies that accessible in the Q band region of the spectrum. The results were used to help interpret both the nature of the electronic transitions in Q band region, and the spectral discrepancies between phthalocyanine and porphyrin systems. © *2012 American Institute of Physics*. [http://dx.doi.org/10.1063/1.3703310]

I. INTRODUCTION

Porphyrin and phthalocyanine complexes form an important class of aromatic dyes, which have been studied extensively in the past decades. In 1930s and 1940s, Linstead and co-workers reported the preparations and UV-Vis spectral data for a number of porphyrin and phthalocyanine complexes, including zinc phthalocyanine (ZnPc) and zinc tetrabenzoporphyrin (ZnTBP) molecules, in a series of papers.[1–6] Since then, lots of experimental and theoretical investigations were performed, initially because of their central role in biological processes such as respiration and photosynthesis,[7] more recently because of their potential technological applications,[8–10] including photovoltaic and solar cells,[11] molecular electronics and photonics, nonlinear optics,[12–14] photodynamic therapy,[15] and so on. These highly stable macrocyclic π-systems display interesting properties such as optical stability and efficient light absorption in the near-infrared and visible region of the spectra that make them potential candidates for applications in optoelectronics, photo conducting materials.[10–14] In view of the possible applications, considerable efforts were devoted to the characterization of electronic structures and spectra of these macrocyclic rings.[16–22] It have been proven to be valuable in designs and fabrications of optical devices.

The intensity and origin of the lowest absorption of macrocyclic rings, the Q and B bands, were widely interpreted by Gouterman's four-orbital model.[23–25] According to the cyclic polyene model for the porphyrin ring, the Q and B bands are derived from the transitions between a pair of highest occupied molecular orbitals, HOMO and HOMO-1(a_{1u} and a_{2u} symmetry), and lowest unoccupied molecular orbital, LUMO (the doubled degenerate e_g symmetry). The strong configuration interaction between the $a_{1u}{}^1e_g{}^1$ and $a_{2u}{}^1e_g{}^1$ excited configuration makes for a low-lying state corresponding to the Q band and a high-lying state corresponding to the B band. The transition dipole moments associated with the configuration mixing result in an anti-parallel and a parallel electron transition, that is to say, lead to a weak absorption (Q band) and a strong absorption (B band). In contrast to the porphyrins, the transition between ground state and the first excited state is fully allowed in phthalocyanines.[25] This fully allowed transition is responsible for the intense and bathochromic shift Q band absorption in the region of 600–850 nm, the so-called therapeutic body window,[15] puts phthalocyanine complexes interrelated with medical

a)Author to whom correspondence should be addressed. Electronic mail: herx@swu.edu.cn.
b)E-mail: cyzhu@mail.nctu.edu.tw.

applications as photosensitize in laser cancer therapy. The redshift and intensification of the *Q* band could be ascribed to the near degeneracy break of HOMO and HOMO-1 orbitals due to the substitution of aza linkages for the methine bridges in the porphyrin macrocycle. That decreases the configuration interaction of $a_{1u}{}^1e_g{}^1$ and $a_{2u}{}^1e_g{}^1$ and removes the forbidden character of electron transition, so the *Q* band absorption in phthalocyanine is much stronger than in porphyrin. In the recently published work implemented by Kobayashi *et al.*,[26] they showed the achievement in designing and synthesizing stable metal phthalocyanines having their main absorption band (*Q* band) beyond 1000 nm. Their outstanding research was premised on acquainting comprehensive information about the electronic structure characters by quantum mechanics calculation and analysis. That stresses the importance of understanding the electronic structure before performing in-depth work about design and synthesis.

Schaffer and his co-workers[17] reported a general symmetrized Extended Hückel program and performed calculations on metal complexes of phthalocyanine. The obtained results were compared with the similar calculations on porphyrins. The molecular orbital model developed by them appears to be in close agreement with the available spectroscopic data. They investigated the similarities and contrasts between porphyrin and phthalocyanine ring systems, found that the bridge nitrogen atoms give rise to $n \rightarrow \pi^*$ transitions, which are probably in the region of the *Soret* band. Extra absorption bands were observed in the near ultra violet region of metal phthalocyanine complexes. Their theoretical work gave a step forward in understanding the electronic structures and electronic spectra of metal complexes of phthalocyanine and porphyrin. Previously, self-consistent-molecular-orbital Pariser-Parr-Pople configuration interaction (SCMO-PPP-CI) (Ref. 27) method was adopted to calculate porphyrin and phthalocyanine systems, the investigation showed the multi-transition excited-states description of phthalocyanine and the pure single $\pi \rightarrow \pi^*$ transition of porphyrin system. Weiss and co-workers[27] in their pioneering work on porphyrins and the related systems showed that Gouterman's four-orbital model is reasonable for the lowest electron transition (*Q* bands) but less reasonable for near ultraviolet transition (*Soret* bands), especially in the case of phthalocyanine that have complicated spectral characterization in *Soret* band region due to additional $n \rightarrow \pi^*$ transitions aroused by azamethine groups.

VanCott and his co-workers published a series papers concerning the optical spectra and magnetic circular dichroism (MCD) spectra for ZnPc and ZnTBP isolated in Argon/matrix over a wide energy range.[28–31] Ziegler and Stillman also reported theoretical investigation of MCD spectra of metal porphyrins and metal phthalocyanines.[32,33] Through the magnetic circularly polarized luminescence, they identified the presence of Jahn-Teller coupling and crystal field splitting on the degenerate first excited singlet state.[33] The application of matrix and its accompanying cryogenic temperatures provided high resolved spectra over the entire region affording a clear characterization of energy and symmetry of excited states. Although spectral band deconvolution analysis and MCD spectra gave indications on the energy, number, and magnetic moment of the excited states contributing to each spectral region, accurate quantum mechanical calculations are still required to fully characterize the excited states.

Recently, Murray and his co-workers investigated visible luminescence spectroscopy, infra-red and Raman spectroscopy of free-base and zinc phthalocyanines isolated in cryogenic matrices.[34,35] Their works offered ample experimental evidences for our theoretical investigation and simulation of the high resolved spectra, and further assigning the vibrational bands involved in spectra of zinc phthalocyanine.

Actually, a compelling need for accurate calculations of the excited states of metal complexes of tetrabenzoporphyrin and phthalocyanine has been expressed already long time ago by VanCott.[28] In order to maximize the quantity and quality of the information that can be obtained from simulated spectra, narrow bands, and well-resolved vibronic structure are required.

Before the advent of time-dependent density functional theory (TDDFT), few density functional theory calculations have been reported due to the inability of offering accurate configuration interaction which characterizes the excited state of metal complexes of phthalocyanine and porphyrins.[36] The TDDFT method has been proved to be an excellent alternative to conventional highly correlated *ab initio* method,[37] such as symmetry adapted cluster configuration interaction (SAC-CI), similarity transformed equation-of-motion coupled cluster, and complete active space self-consistent-field plus second-order perturbation theory, as in the case of magnesium porphyrin (MgP)[38,39] and magnesium porphyrazine (MgPz).[40] The DFT combined with multireference configuration interaction (DFT/MRCI) method has successfully applied in the calculation of electronic spectra of porphyrins, metal porphyrins, porphyrazines and hydroporphyrins.[41] The reliability of TDDFT method in obtaining accurate predictions of excitation energies and oscillator strengths is by now well documented for a wide range of molecules, ranging from small molecules to large organic molecules, free-base porphine, and transition metal tetrapyrrole complexes.[37] Grimme and his co-workers performed the first time calculations employing the (TD)DFT method and the popular B3-LYP functional to simulate the vibronic structure of the absorption spectra for several large organic π systems. Their pioneering works provide valuable guidance for the following investigations.[42]

In order to afford a reliable description of the electronic spectra that is competitive in accuracy with experimental data, we should perform a calculation of Franck-Condon factors (FCFs) of various peaks in vibronic spectra, oscillator strengths, and excitation energies. The distribution of FCFs among vibrational states reflects information about molecular structures.[43] Take transition from the vibronic ground state to the first singlet excited state as an instance. The equilibrium structures of the two electronic states are semblable if the origin band has a maximum FCF close to unity, whereas if the maximum FCF shifts to some vibrational states that are highly excited, then the two states are likely to have quite different geometries. Moreover, the active vibrational modes with larger FCFs usually indicate that the corresponding geometric parameters (e.g., bond lengths or bond angles) change drastically upon excitation. So it is necessary to perform a comprehensive vibrational mode analysis involved in the optical

spectra. Lots of theoretical studies of excited states reported in the literatures consider only vertical excitation energies in the Franck-Condon region.[33,37,44] However, weak electron transition, such as the $S_0 \leftrightarrow S_1$ ($\pi \rightarrow \pi^*$) transition in porphyrin systems, often exhibits vibronic activity. To comprehend the activity, it is indispensable to beyond the Born-Oppenheimer approximant and to consider the dependence of the electronic transition moment. Usually, it is a difficult task to accurately calculate the FCFs due to the complexity of such a calculation owes itself to the fact that the normal modes in an excited state generally could not only be distorted (having different frequencies) and displaced (having different equilibrium geometries) but also be mixed (having different characters of normal modes, generally called the Duschinsky effect) with each other, which makes the calculations of the vibrational overlap integrals between ground- and excited-state normal coordinates challenging,[45] especially for large molecule, such as zinc complexes of phthalocyanine (165 normal modes) and tetrabenzoporphyrin (177 normal modes).

The recent developments in electronic theories and methods and the increasing computation power allow nowadays accurately treating systems of medium and large sizes.[42,46–51] Previously, the optical spectra of sizable molecules were simulated with the linear coupling model by Domcke *et al.*[52] However, this procedure is affordable for a reasonable description of the low resolved spectra. It is defective to characterize the spectra features and provide a direct link between spectra and structural parameters. In this present paper, we described a study of absorption and fluorescence spectra of ZnPc and ZnTBP in the region of *Q* states. Very strong similarities are notable compared with previous experimental studies. A key aspect of the present work is the exploitation of the vibrational analysis to obtain assignments for the emission and absorption bands. Moreover, detailed comparisons between emission and absorption were carried out, which aids considerably in the identification of the true band assignments in the region of *Q* states.

II. COMPUTATIONAL METHODS AND THEORETICAL DETAILS

A. Computational methods

Guthmuller and co-workers investigated the resonance Raman properties and absorption spectra of julolidinemalononitrile push-pull chromophore with different functional.[53] The studied results indicated that the amount of Hartree-Fock (HF) exchange in the hybrid functional should have a great impact on the calculated results, which is in agreement with previous investigations performed by Grimme and his co-workers.[46,54] They reported that the vibronic structure critically depends on the fractions of the "exact" Hartree-Fock exchange included in hybrid functionals. This can be traced back to the important effect of "exact" Hartree-Fock exchange on the geometrical displacement upon excitation. In the present work, therefore, equilibrium geometries and their vibrational-normal-mode frequencies of their ground and first excited states of ZnPc and ZnTBP were calculated by using three different hybrid exchange correlation functionals, B3LYP, PBE0, and BHandHLYP containing 20%, 25%, and 50% of exact HF exchange of the density functional theory and its time-dependent extension methods. This choice of functional was consistent with recent benchmark calculations that demonstrated,[46,53,54] depending on the selected molecule, B3LYP could be the most efficient approaches amongst the three functional, at least for the low lying $\pi \rightarrow \pi^*$ transition. In this work, the results calculated by B3LYP functional were adopted to compare with the previous theoretical and experimental data, and those of the other two functional were given in the supplementary material.[73] The triple zeta valence basis set augmented with polarization function (def-TZVP) was used for all atoms. The def-TZVP basis set is comprised of four basis function for H atom (5*s*1*p*)/[3*s*1*p*], nine basis function for C and N atoms (11*s*6*p*1*d*)/[5*s*3*p*1*d*] and 13 basis function for Zn atom (17*s*11*p*6*d*)/[6*s*4*p*3*d*]. The terms in parentheses and square brackets represent numbers of primitive and contracted basis function, respectively. The ground states and the first singlet excited states of ZnPc and ZnTBP were optimized under D_{4h} and D_{2h} point group symmetry constraint, respectively. Frequency calculations at the same level were performed to confirm each stationary point to be a true energy minimum (all frequencies are presented in the supplementary material[73]). The choice of E_u irreducible representation of electronic state depends on the choice of Cartesian axes. For the consistencies with experimental results and make our calculations reliable, the ZnPc and ZnTBP molecules were placed in *xy*-plane with *z*-axis to be perpendicular to the molecular plane and then the C_4 axis was chosen as *x*-axis, as shown in Fig. 1. In this way, we determined the first singlet excited states were doubly degenerate with E_u symmetry label for ZnPc and ZnTBP. In order to determine whether the existence of the electronic origin in the high energy shadow of peak *Q*, which stems from the *n* (N_m lone pairs) $\rightarrow \pi^*$ transitions, we performed the analysis of individual atom contribution to the molecular orbitals (MOs) of ZnPc.

All geometries optimizations, frequency calculations of ground- and excited-states for ZnPc and ZnTBP, transition dipole moment derivatives and the analysis of individual atom contribution to the MOs were performed in the TURBOMOLE 6.2 software package.[55]

The vibrationally resolved absorption and fluorescence spectra including Duschinsky[56] and Herzberg-Teller[57] contributions were simulated based on the accurate calculations of equilibrium geometries and their vibrational-normal-mode frequencies of the ground and their first excited states with our own code and FCclasses program.[58]

B. General theory of molecular spectra

The absorption coefficient for the electronic transition $m \rightarrow n$ in the Condon approximation can be expressed as[45]

$$a(\omega) = \frac{4\pi^2\omega}{3\hbar c} |\vec{\mu}_{nm}|^2 \sum_{\nu} \sum_{\nu'} P_{m\nu} |\langle \Theta_{n\nu'} | \Theta_{m\nu} \rangle|^2 \times \delta(\omega_{n\nu',m\nu} - \omega) \quad (1)$$

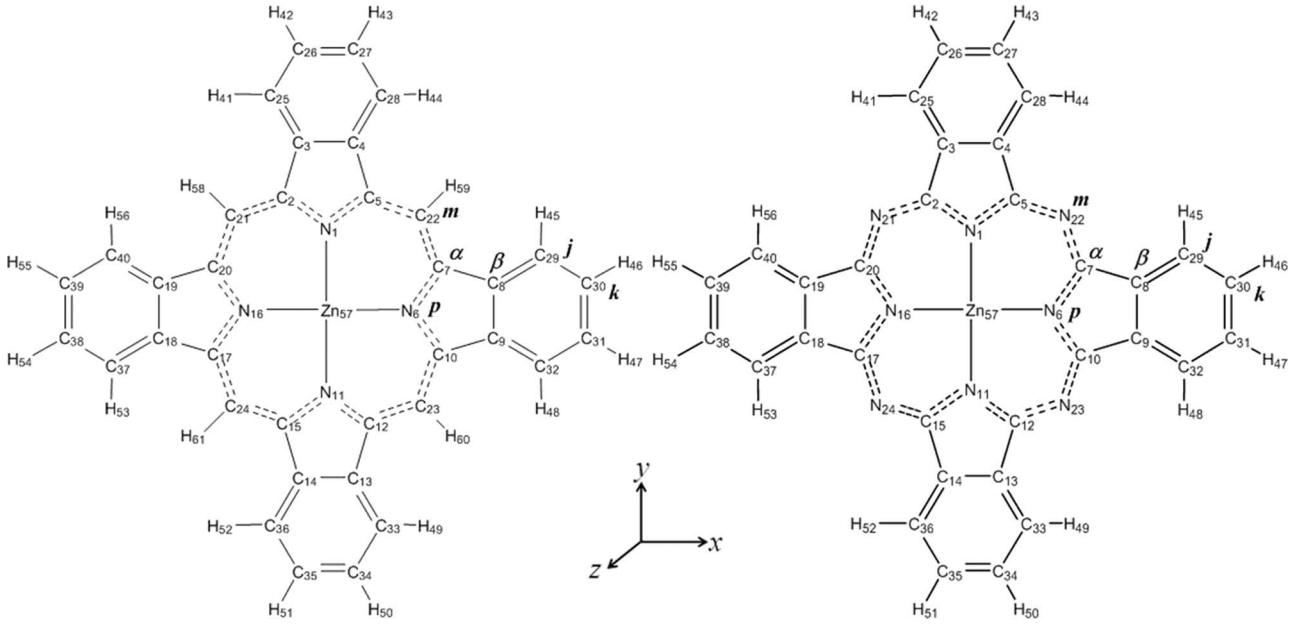

FIG. 1. Molecule structures of zinc complexes of tetrabenzoporphyrin (ZnTBP, left) and phthalocyanine (ZnPc, right).

In which $\delta\left(\omega_{n\nu',m\nu}-\omega\right)$ is the Lorentzian line-shape function, $P_{m\nu}$ denotes the Boltzmann factor, c is the speed of light, $|\langle\Theta_{n\nu'}\mid\Theta_{m\nu}\rangle|^2$ is the Franck-Condon factor, and $\vec{\mu}_{nm}$ is the electronic transition dipole moment. Eq. (1) can be rewritten as

$$a(\omega)=\frac{4\pi^2\omega}{3\hbar c}|\vec{\mu}_{nm}|^2\int_{-\infty}^{\infty}dt\exp\left[it\left(\omega_{nm}-\omega\right)\right]\cdot G(t) \tag{2}$$

Here, $G(t)$ denotes the correlation function and is given by

$$G(t)=\sum_{\nu}\sum_{\nu'}P_{m\nu}\,|\langle\Theta_{n\nu'}\mid\Theta_{m\nu}\rangle|^2\exp\left[\frac{it}{\hbar}(E_{n\nu'}-E_{m\nu})\right] \tag{3}$$

Let us consider the general case, that is, a molecular system consists of N_d modes exhibiting the Duschinsky effect and N modes without mode mixing. In this case, $G(t)$ can be written as[45]

$$G(t)=G_{1,2,\ldots,N_d}(t)\prod_{l}^{l\neq1,2,\ldots,N_d}G_l(t) \tag{4}$$

$G_{1,2,\ldots,N_d}(t)$ and $G_l(t)$ denote the correlation functions defined by

$$G_l(t)=\sum_{\nu l}\sum_{\nu' l}P_{m\nu_l}|\langle\chi_{n\nu'_l}(Q'_l)\mid\chi_{m\nu_l}(Q_l)\rangle|^2\times\exp\left[it\left\{\left(\nu'_l+\frac{1}{2}\right)\omega'_l-\left(\nu_l+\frac{1}{2}\right)\omega_l\right\}\right] \tag{5}$$

and

$$G_{1,2,\ldots,N_d}(t)=\sum_{\nu_1}\cdots\sum_{\nu_{N_d}}\sum_{\nu'_{\alpha1}}\cdots\sum_{\nu'_{\alpha N_d}}P_{m\nu_1\cdots\nu_{Nd}}|\langle\chi_{n\nu'_{\alpha1}}(Q'_{\alpha_1})\cdots\chi_{n\nu'_{\alpha Nd}}(Q'_{\alpha_{Nd}})\times\mid\chi_{m\nu_1}(Q_1)\cdots\chi_{m\nu_{Nd}}(Q_{N_d})\rangle|^2\times\exp\left[it\left\{\sum_{\alpha=\alpha_1}^{\alpha N_d}\left(\nu'_\alpha+\frac{1}{2}\right)\omega'_\alpha-\sum_{j=1}^{N_d}\left(\nu_j+\frac{1}{2}\right)\omega_j\right\}\right]. \tag{6}$$

That is, $G_{1,2,\ldots,N_d}(t)$ represents the correlation function of the mixing modes (i.e., the Duschinsky effect).

Making use of the Slater sum, we obtain

$$G_{1,2,\ldots,N_d}(t)=\prod_{j=1}^{N_d}\left\{\frac{2\sqrt{\beta_j}\sinh\frac{\hbar\omega_j}{2kT}}{\sqrt{2\pi\sinh\lambda_j}}\right\}\prod_{\alpha=\alpha_1}^{\alpha_{N_d}}\left\{\frac{\sqrt{\beta'_\alpha}}{2\pi\sinh\mu'_\alpha}\right\}\times\prod_{j=1}^{N_d}\left\{\int_{-\infty}^{\infty}dQ_j\int_{-\infty}^{\infty}d\bar{Q}_j\right\}\times\exp\left[-\sum_{j=1}^{N_d}\frac{\beta_j}{4}\left\{(Q_j+\bar{Q}_j)^2\tanh\frac{\lambda_j}{2}+(Q_j-\bar{Q}_j)^2\coth\frac{\lambda_j}{2}\right\}\right]\times\exp\left[-\sum_{\alpha=\alpha_1}^{\alpha_{N_d}}\frac{\beta'_\alpha}{4}\left\{(Q'_\alpha+\bar{Q}'_\alpha)^2\tanh\frac{\mu'_\alpha}{2}+(Q'_\alpha-\bar{Q}'_\alpha)^2\coth\frac{\mu'_\alpha}{2}\right\}\right], \tag{7}$$

where $\beta_j = \omega_j/\hbar$, $\beta_\alpha = \omega'_\alpha/\hbar$, $\lambda_j = it\omega_j + \hbar\omega_j/(kt)$, $\mu_\alpha = -it\omega'_\alpha$, and

$$Q'_\alpha = \sum_{j=1}^{N_d} C_{\alpha j}(Q_j + \Delta Q_j), \tag{8}$$

for $\alpha = \alpha_1, \ldots, \alpha_{N_d}$, it follows that

$$G_{1,2,\ldots,N_d}(t) = e^{-D} \prod_{j=1}^{N_d} \left\{ \frac{2\sqrt{\beta_j}\sinh\frac{\hbar\omega_i}{2kT}}{\sqrt{2\pi\sinh\lambda_i}} \right\} \times \prod_{\alpha=\alpha_1}^{\alpha_{N_d}} \left\{ \frac{\sqrt{\beta'_\alpha}}{\sqrt{2\pi\sinh\mu'_\alpha}} \right\} \prod_{j=1}^{N_d} \left\{ \int_{-\infty}^{\infty} dQ_j \int_{-\infty}^{\infty} d\bar{Q}_j \right\}$$
$$\times \exp\left[-\sum_{j=1}^{N_d} A_{jj}(Q_j + \bar{Q}_j)^2 - \sum_{j=1}^{N_d}\sum_{k>j}^{N_d} A_{jk}(Q_j + \bar{Q}_j)(Q_k + \bar{Q}_k) \right] \times \exp\left[-\sum_{j=1}^{N_d} A_j(Q_j + \bar{Q}_j) \right]$$
$$\times \exp\left[-\sum_{j=1}^{N_d} B_{jj}(Q_j - \bar{Q}_j)^2 - \sum_{j=1}^{N_d}\sum_{k>j}^{N_d} B_{jk}(Q_j - \bar{Q}_j)(Q_k - \bar{Q}_k) \right], \tag{9}$$

where

$$A_{jj} = \frac{\beta_j}{4}\tanh\frac{\lambda_j}{2} + \sum_{\alpha=\alpha_1}^{\alpha_{N_d}} \frac{\beta'_\alpha}{4}\tanh\frac{\mu'_\alpha}{2}(C_{\alpha j})^2, \tag{10}$$

$$A_{jk} = \sum_{\alpha=a_1}^{\alpha_{N_d}} \frac{\beta'_\alpha}{2}\tanh\frac{\mu'_\alpha}{2} C_{\alpha j} C_{\alpha k}, \tag{11}$$

$$A_j = \sum_{\alpha=\alpha_1}^{\alpha_{N_d}}\sum_{k=1}^{\alpha_{N_d}} \beta'_\alpha \tanh\frac{\mu'_\alpha}{2} C_{\alpha j} C_{\alpha k}\Delta Q_k, \tag{12}$$

$$B_{jj} = \frac{\beta_j}{4}\coth\frac{\lambda_j}{2} + \sum_{\alpha=\alpha_1}^{\alpha_{N_d}} \frac{\beta'_\alpha}{4}\coth\frac{\mu'_\alpha}{2}(C_{\alpha j})^2, \tag{13}$$

$$B_{jk} = \sum_{\alpha=\alpha_1}^{\alpha_{N_d}} \frac{\beta'_\alpha}{2}\coth\frac{\mu'_\alpha}{2} C_{aj} C_{ak}, \tag{14}$$

and

$$D = \sum_{\alpha=\alpha_1}^{\alpha_{N_d}} \beta'_\alpha \tanh\frac{\mu'_\alpha}{2}\left(\sum_{j=1}^{N_d} C_{\alpha j}\Delta Q_j \right)^2 \tag{15}$$

Next, we shall calculate $G_l(t)$ given by Eq. (5) for the displaced and distorted harmonic oscillator case. It is given by

$$G_l(t) = \frac{2\beta_l\beta'_l\sinh\frac{\hbar\omega_l}{2kT}}{\sqrt{\left(\beta_l\tanh\frac{\lambda_l}{2} + \beta'_l\tanh\frac{\mu'_l}{2}\right)\left(\beta_l\coth\frac{\lambda_l}{2} + \beta'_l\coth\frac{\mu'_l}{2}\right)}}$$
$$\times \exp\left[-\frac{\beta_l\beta'_l\Delta Q_l^2}{\beta_l\coth\frac{\mu'_l}{2} + \beta'_l\coth\frac{\lambda_l}{2}} \right] \tag{16}$$

The electronic transition dipole moments $\vec{\mu}_{nm}$ depend on the nuclear coordinates. In order to obtain more reasonable electronic spectra, the transition dipole moment is expanded in a Taylor series in terms of the nuclear coordinate,

$$\vec{\mu}_{nm} = \vec{\mu}_{nm}(0) + \left(\frac{\partial\vec{\mu}_{nm}}{\partial Q}\right)_0 Q + \cdots \tag{17}$$

The zero-order term of this expansion is generally referred as the FC approximation for strongly allowed transitions, while the first-order term is the so-called Herzberg-Teller (HT) effect for weakly allowed or forbidden transition. In the present work, the vibrationally resolved spectra of ZnPc and ZnTBP including the HT and Duschinsky contributions were computed. The spectra were simulated with a full width at half maximum (FWHM) of 0.0005 eV. The maximum number of integrals to be computed for each class was set to 10^6. The simulated spectrum taking into account both the zero-order (FC) and the first-order (HT) terms of Eq. (17) will be named as FCHT. In order to investigate the HT and Duschinsky contributions separately, the Figures of pure HT contribution and the summation of HT and Duschinsky contributions were plotted.

III. RESULTS AND DISCUSSION

A. Geometrical and electronic structures

The accuracy of the simulated optical spectra is dependent upon the electronic structural parameters used in the simulation, it is crucial to verify the quality of the optimized structures by comparing them with available experimental data. For the well-resolved $S_0 \leftrightarrow S_1$ absorption and fluorescence spectra of ZnTBP and ZnPc, the good optimizations of ground state and the first excited singlet state should be essential prerequisite. Although the equilibrium geometries of the ground states of ZnTBP and ZnPc were well studied in theory and experiment,[44,59,60] the investigations of their first excited singlet states were still very limited. The calculated key geometrical parameters of the ground states and the excited states of ZnTBP and ZnPc were listed in Table I. The calculated results of ZnTBP are in good agreement with the previously theoretical data.[44,59] For ZnPc, the

TABLE I. Calculated bond lengths (Å) and angles (degree) for the first singlet excited states of ZnPc and ZnTBP with B3LYP/def-TZVP.

	ZnTBP				ZnPc		
Parameter	S_0	Calc.[a]	S_1	Parameter	S_0	Expt.[b]	S_1
Zn_{57}-N_6	2.0775	2.078	2.0765	Zn_{57}-N_6	2.0028	1.980	2.0001
Zn_{57}-N_1	2.0775	2.078	2.0783	Zn_{57}-N_1	2.0028	1.980	2.0035
C5-C22	1.3882	1.391	1.3985	C5-N22	1.3268	1.331	1.3417
C7-N6	1.3702	1.374	1.3765	C7-N6	1.3688	1.369	1.3759
C7-C22	1.3882	1.391	1.3854	C7-N22	1.3268	1.331	1.3200
C7-C8	1.4535	1.455	1.4571	C7-C8	1.4604	1.455	1.4658
C8-C9	1.4074	1.411	1.4075	C8-C9	1.4082	1.400	1.4063
C8-C29	1.3968		1.3930	C8-C29	1.3912	1.393	1.3870
C29-C30	1.3862		1.3915	C29-C30	1.3902	1.399	1.3969
C30-C31	1.4050		1.4002	C30-C31	1.4032	1.396	1.3973
Zn57-N6-C7	125.639		125.778	Zn57-N6-C7	124.981	125.4	125.067
N6-C7-C22	125.504	125.4	125.577	N6-C7-N22	127.411	127.8	127.776
C7-C22-C5	127.715	127.3	127.457	C7-N22-C5	125.216		124.663
C5-N1-C2	108.723	108.0	108.522	C5-N1-C2	110.039	109.1	109.861
N1-C2-C3	109.261	109.7	109.375	N1-C2-C3	108.372	108.8	108.479
C4-C3-C2	106.378	106.2	106.364	C4-C3-C2	106.608	106.6	106.591
C4-C3-C25	120.625		120.516	C4-C3-C25	120.998		120.829
C3-C25-C26	118.433		118.561	C3-C25-C26	117.859	117.3	118.048
C25-C26-C27	120.942		120.923	C25-C26-C27	121.142	121.5	121.123

[a]The calculated data with B3LYP/6-31G* level by Nguyen *et al.*[44,59]
[b]The x-ray data reported by Scheidt and Dow.[60]

calculated geometrical parameters are consistent with the x-ray data, which reported by Scheidt and Dow.[60] The ground structures of ZnPc and ZnTBP are found to have D_{4h} symmetry at the same level of theory. The Zn_{57}-N_6 (2.0028 Å) distance of ZnPc is slightly overestimated by 0.0228 Å than experimental value (1.980 Å); the C-N and C-C distances are well within 0.01 Å of the experimental values. The bond angles are within one degree of experimental data.[60] Compared the square structure of ZnPc with ZnTBP, we found that the Zn-N distance is shorter for ZnPc, and the C_7-N_6 (1.3688 Å) and C_7-N_{22} (1.3268 Å) distances of ZnPc are also slightly shorter than C_7-N_6 (1.3702 Å) and C_7-C_{22} (1.3882 Å) in ZnTBP. From the comparison above, we could find that the size of the central hole is reduced from ZnTBP to ZnPc due to the nitrogen substitutions of the four *meso* positions. That result tallies with the previous reports.[44,59,61,62] The first singlet excited states (S_1) of ZnPc and ZnTBP are doubly degenerate with E_u symmetry. The D_{4h} square structure of the ground state is expected to distort into a D_{2h} rectangle due to the existing of Jahn-Teller effects. We noted that the lowest singlet excited state of ZnPc largely originates from the HOMO ($2a_{1u}$) → LUMO ($7e_g$) (93%) excitation from the ground state. The degenerate e_g orbital gives rise to the b_{2g} and b_{3g} orbitals, a_{1u} transfers to a_u under D_{2h} symmetry. So the geometry optimization for the first singlet excited state of ZnPc system leads to the rectangular structures of $^1B_{2u}$ ($a_u \otimes b_{2g}$) and $^1B_{3u}$ ($a_u \otimes b_{3g}$) electronic states. Similarly, the lowest singlet excited state of ZnTBP is derived from the HOMO ($2a_{1u}$) → LUMO ($7e_g$) (77.9%) and HOMO-1 ($6a_{2u}$) → LUMO ($7e_g$) (21.6%), the a_{1u} and a_{2u} irreducible representations transform to a_u and b_{1u} under D_{2h} symmetry, respectively. Therefore, the optimizations for the first singlet excited state of $^1B_{2u}$ ($a_u \otimes b_{2g}$, $b_{1u} \otimes b_{3g}$) and $^1B_{3u}$ ($a_u \otimes b_{3g}$, $b_{1u} \otimes b_{2g}$) states were performed. The B_{2u} and B_{3u} states are expected to be near in energy, it was confirmed by our TD calculations. Structurally, the geometrical changes upon going from S_0 to S_1 involved primarily the C_α-C_β, C_β-C_β, C_m-C_β, and Zn-N bonds. The principal (in-plane) C_2 axis bisects the β carbons of the distorted excited state structure for the rectangle. For ZnPc, the Zn_{57}-N_6 distance is decreased to 2.0001 Å compared with the ground state, and the Zn_{57}-N_1 distance is lengthened to 2.0035 Å. The C_7-N_6 and C_5-N_{22} distances are prolonged to 1.3759 Å and 1.3417 Å, respectively, while the C_7-N_{22} is shortened in the S_1 state. The scenes also can be seen for ZnTBP, the Zn_{57}-N_6 distance is decreased while Zn_{57}-N_1 is prolonged respected to the ground state. The C_5-C_{22} and C_7-N_6 distances are lengthened to 1.3985 Å and 1.3765 Å, C_7-C_{22} was slightly shortened.

We calculated the vertical excitation energies and the corresponding oscillator strengths of the first three excited singlet states estimated at equilibrium geometries of ZnPc and ZnTBP ground states with B3LYP, PBE0, and BHandHLYP functionals. As shown in Table II, for S_1 ($1E_u$) of ZnPc, the calculated vertical excitation energy and oscillator strength with B3LYP functional are 2.08 eV and 0.429, respectively. The corresponding experimental excitation energies are 1.95 (Ref. 63) and 1.89 (Ref. 28) eV, oscillator strength is 0.4.[64] The excitation energies calculated with the PBE0 and BHandHLYP functionals are 2.12 eV and 2.10 eV, which are comparative with the result of B3LYP. But the oscillator strengths are much higher than the results from B3LYP calculation and experimental measurements.[28,63] These scenes are pretty alike for ZnTBP molecule. From above comparisons, we could conclude that the increasing amount of "exact" Hartree-Fock exchange included in the functionals is mainly

TABLE II. Calculated vertical transition energy (ΔE, unit is eV) and oscillator strengths (f) of ZnPc and ZnTBP from S_0 to S_1 together with the experimental and previously theoretical data.

	B3LYP				PBE0		BHandHLYP			
	def-TZVP		6-31G*[a]		def-TZVP		def-TZVP		Expt.	
ZnPc	E	f	E	f	E	f	E	f	E	f
$1E_u$	2.08	0.429	2.09	0.418	2.12	0.456	2.10	0.537	1.95[b], 1.89[c]	0.40[d]
$2E_u$	3.37	0.008	3.37	0.008	3.54	0.007	4.08	0.000		
$3E_u$	3.66	0.148	3.66	0.172	3.85	0.230	4.39	1.156	3.71[b], 3.71[c]	
ZnTBP										
$1E_u$	2.16	0.175	2.18	0.173	2.22	0.188	2.22	0.233	2.06[e],1.98[d]	0.17[f]
$2E_u$	3.25	1.136	3.28	1.121	3.35	1.201	3.61	1.408	3.18[e],3.06[d]	0.92[f]
$3E_u$	3.72	0.126	3.78	0.128	3.84	0.111	4.33	0.064		

[a]Theoretical data carried out under B3LYP with 6-31G* basis set.[59]
[b]Data taken in gas-phase supersonic jet.[63]
[c]Data taken in an Ar matrix.[28]
[d]Data taken in gas-phase.[62]
[e]Data taken in gas-phase supersonic jet.[66]
[f]Data reported by Linstead *et al.*[64]

responsible for intensification and a shift of the 0-0 transition to the higher energy region. This modification is associated with an increase of the geometric displacement upon excitation, which is in accord with previous findings.[46,54] However, compared ZnPc with ZnTBP, there are obvious contrasts in the vertical excitation energies and the oscillator strengths. These contrasts we predicted also can be seen in other works.[40,59,61,65] For S_1, the oscillator strength of ZnPc ($f = 0.429$) is much higher than ZnTBP ($f = 0.175$) and the excitation energy of ZnPc ($\Delta E_1 = 2.08$ eV) is lower than ZnTBP ($\Delta E_1 = 2.16$ eV). The increase of oscillator strength and the decrease of excitation energy could be reflected with the intensification and redshift of the Q band of ZnPc. That could be ascribed to the substitution of aza linkages for the methine bridges in the porphyrin macrocycle. The substitution decreases the configuration interaction of $a_{1u}{}^1e_g{}^1$ and $a_{2u}{}^1e_g{}^1$ and removes the forbidden character of electron transition, so the Q band absorption in ZnPc is much stronger than in ZnTBP. Furthermore, the substitution could dramatically stabilize the LUMO orbital although it can lead to destabilization of the HOMO, the energy drop of LUMO is 0.6507 eV and the energy enhance of HOMO is 0.3243 eV. The contrast of stabilizing and destabilizing energies would make for the decrease of vertical excitation energy. Moreover, the nitrogen substitutions for the methine bridges bring on the decrease of the size of central hole compared to the ZnTBP,[44,59] as demonstrated by our calculated geometrical parameters (see Table I). The decrease of the central hole size could strengthen the interaction between central metal atom and Pc ligands (C and N, the elements that constitute the Pc ligands) and stabilize the excited state relative to the ground state.[26] It provided the concept of taking the size of central hole into account for designing geometrical structure and further adjusting the absorption wavelengths.

For the B band, the TD calculations for ZnTBP molecule predicted a single band at 3.25 eV with oscillator strength of 1.136, which are in agreement with the theoretical results from Nguyen *et al.*,[59] and the corresponding experimental data obtained in a supersonic jet expansion (3.18 eV) (Ref. 66) and in the gas-phase (3.06 eV).[62] The B band of ZnTBP is assigned to the $2E_u$ state, which is made up of the HOMO ($2a_{1u}$) →LUMO ($7e_g$) (72.7%) and HOMO-1 ($6a_{2u}$) → LUMO ($7e_g$) (19.9%). For ZnPc, the B band and higher energy regions are much more complex. The $2E_u$ state located at the tail of the B bands with a very small oscillator strength ($f = 0.008$) is hardly observed in experiment. The $2E_u$ state mainly stems from the HOMO-1($3b_{2u}$) → LUMO ($7e_g$) (91.6%). In the present work, the B band of ZnPc is assigned to the $3E_u$ (not $2E_u$) with the oscillator strength of 0.148, the excitation energy (3.66 eV) of $3E_u$ calculated with B3LYP is just slightly underestimated compared to the experimental value (3.71 eV). These results are in accordance with the published work from Nguyen *et al.*[59]

B. Simulated versus experimental optical spectra

The well-resolved spectra and assignments of the involved vibrational modes of ZnPc and ZnTBP molecules were presented here. It is known that the $S_0 \leftrightarrow S_1$ electron transition (Q band) of ZnPc is much stronger than ZnTBP as predicted by our vertical transition calculations. In the simulations of $S_0 \leftrightarrow S_1$ spectra, the HT and Duschinsky contributions were expected to be important for ZnTBP and ZnPc. The HT effect including Duschinsky mixing (labeled HT) to the spectra of ZnTBP and ZnPc was calculated. In addition, the pure HT (labeled HT') contribution to ZnTBP and ZnPc spectra was also calculated and the plotted figures were presented in Fig. 2. It could give a visualized sight of the HT and Duschinsky contributions in the simulated spectra. Luo and co-workers performed an investigation on absorption spectrum of porphine,[67] which included the HT effects but neglected both the Duschinsky coupling and the changes in the frequencies of the normal modes in the two electronic states. However, the simultaneous consideration of Duschinsky and HT couplings is necessary to account exactly for the role of nuclear vibrations in an optical transition,[68] especially for the sizable molecules. In the FC spectrum,

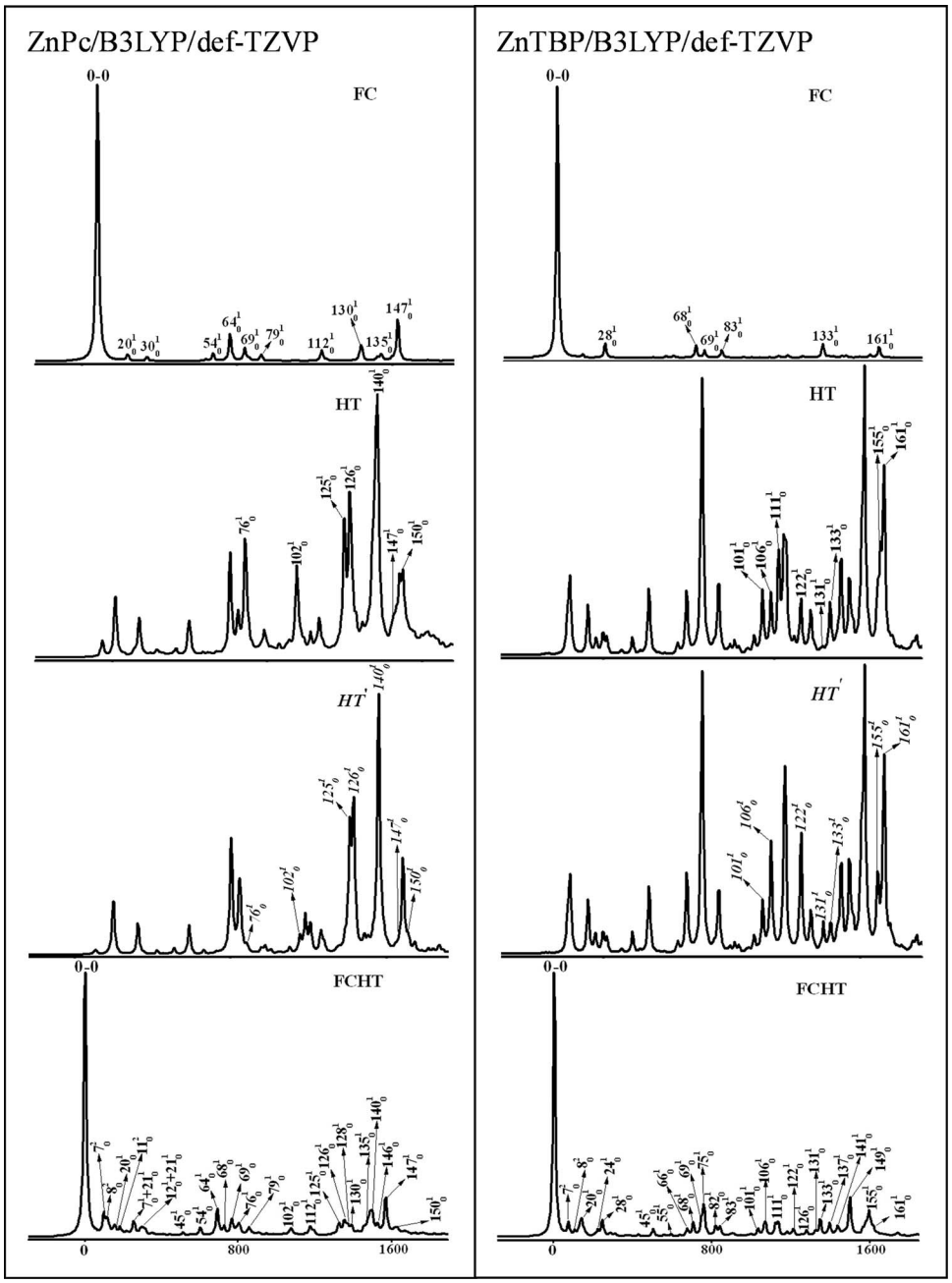

FIG. 2. Simulated well-resolved absorption spectra of ZnPc and ZnTBP, calculated with B3LYP/def-TZVP, within a range of about 1630 cm^{-1} from the 0-0 transition frequency (set to zero). The simulated spectra taking into account both the zero-order (FC) and the first-order (HT) terms of Eq. (17) will be named as FCHT. *HT'* represents pure Herzberg-Teller effects and HT represents summation of Herzberg-Teller effects and Duschinsky effects.

in order to confirm that the displaced harmonic oscillator is good approximation to be used for simulating the optical spectrum, it requires that the difference between vibrational frequencies of S_0 and S_1 states must be small for each totally symmetric (a_g, under D_{2h} point group symmetry) vibrational normal mode of the investigated molecules. For example, the frequency differences of the totally symmetric modes of ZnPc, ν_{20}, ν_{30}, ν_{54}, ν_{64}, ν_{69}, ν_{79}, ν_{112}, ν_{130}, ν_{135}, and ν_{147}, for S_0 and S_1 states, are about 0.93, 0.87, 3.0, 3.5, 4.1, 0.62, 3.1,,13, 6.3, and 0.98 cm^{-1}, respectively. The situation is also similar to ZnTBP molecule. According to the above analysis, we considered that the displaced harmonic oscillator approximation is reasonable to simulate the optical spectra.

1. The absorption and fluorescence spectra of ZnPc

The FC and FCHT well-resolved optical spectra of ZnPc were simulated (absorption and fluorescence spectra were presented in Figs. 2 and 3, respectively). Compared with the experimental absorption spectra reported by VanCott *et al.*[28] and Murray *et al.*,[35] the FCHT spectrum showed the full profile of *Q* band, the intensities relative to the 0-0 transition were collected in Table III. Three major band envelopes were reproduced, traditionally labeled *Q* (0, 0), *Q* (1, 0), *Q* (2, 0),[28] as shown in Fig. 4. Based on the experimental data,[28,35] we assigned the locations of involved vibrational modes in FC and FCHT spectra. From the simulated spectra, we can see

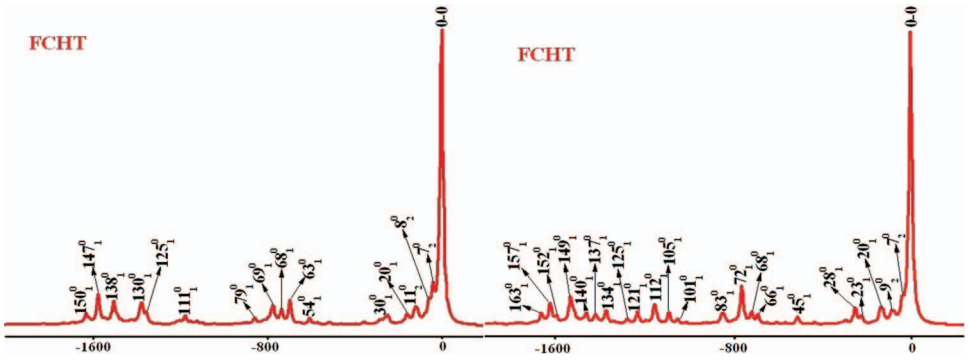

FIG. 3. Simulated well-resolved FCHT fluorescence spectra of ZnPc (left) and ZnTBP (right) with B3LYP/def-TZVP.

the spectral profile is dominated by the 0-0 transition. This result implied only small displacement of the position of a minimum on the potential energy surface between the ground- and excited-states was generated. The Q (0, 0) envelope can be accounted for by the presence of three involved modes with frequencies 154 cm^{-1}, 225 cm^{-1}, and 252 cm^{-1} in VanCott's work (as presented in Table III).[28] But in our simulation, there are six modes interrelated with the Q (0, 0) envelope. Their frequencies are 97.26, 114.38, 157.27, 180.96, 252.15, and 311.91 cm^{-1}. The nearest vibrational band to the 0-0 origin with the frequency 87 cm^{-1} was reported recently by Murray *et al.*,[35] which is physically consistent with our 97.26 cm^{-1}. The extra modes with 114.38 and 180.96 cm^{-1} are derived from the fundamental $0 \rightarrow 1$ transition of modes

TABLE III. Relevant normal modess of the electronic states in the FCHT absorption spectrum of ZnPc, calculated with B3LYP/def-TZVP.

State S_1				State S_0					
n[a]	ω[b]	i[c]	δ[d]	$m'1$[e]	$m'2$[e]	$m'3$[e]	$\Delta\omega$[f]	ω_{exp}[g]	ω_{exp}[h]
7^2	97.26	7.5	0.000	7′[0.98]	19′[0.01]	25′[0.01]	29.00		87
8^2	114.38	4.3	0.000	8′[0.96]	13′[0.03]	27′[0.00]	28.14		
20^1	157.27	2.6	0.225	20′[1.00]			− 0.93	154	154
11^2	180.96	1.6	0.000	11′[0.99]	22′[0.01]		23.18	225	225
$21^1 + 7^1$	252.15	2.7	0.000	25′[0.80]	19′[0.13]	27′[0.02]	3.62	255	252
$12^1 + 21^1$	311.91	1.4	0.000	19′[0.86]	25′[0.13]	35′[0.01]	− 16.27		
45^1	506.86	1.0	0.000	45′[1.00]			− 4.36	479	478
54^1	598.43	2.9	0.236	54′[1.00]			− 2.96	589	586
64^1	686.23	9.8	0.430	63′[1.00]			− 3.52	676	675
68^1	722.80	3.2	0.000	68′[0.94]	75′[0.06]		− 5.96	739	742
69^1	761.31	5.0	− 0.308	69′[1.00]			− 4.05		
76^1	801.89	3.0	0.000	75′[0.71]	70′[0.24]	68′[0.04]	27.06		
79^1	851.16	2.3	0.206	79′[1.00]			− 0.62	840	851
102^1	1069.96	2.5	0.000	103′[0.90]	108′[0.05]	113′[0.03]	− 1.79		
112^1	1168.75	3.0	0.247	111′[0.98]	115′[0.01]	112′[0.00]	3.05	1133	
125^1	1319.18	2.3	0.000	120′[0.39]	125′[0.32]	126′[0.24]	0.94	1334	
126^1	1345.69	4.5	0.000	126′[0.45]	125′[0.35]	128′[0.11]	2.67	1350	
128^1	1365.12	2.0	− 0.192	129′[0.93]	123′[0.03]	131′[0.02]	− 1.49		
130^1	1385.05	2.6	− 0.221	130′[0.98]	123′[0.01]	136′[0.00]	12.96	1408	
135^1	1448.86	4.0	0.193	134′[0.93]	131′[0.03]	136′[0.01]	− 6.26	1466	
140^1	1491.39	6.0	0.000	138′[0.58]	144′[0.28]	145′[0.10]	− 7.83	1500	
146^1	1518.98	3.1	0.237	146′[0.90]	147′[0.08]	131′[0.01]	− 10.08		
147^1	1560.35	13.5	0.494	147′[0.88]	146′[0.09]	134′[0.01]	− 0.98	1565	
150^1	1628.14	1.3	0.000	155′[0.57]	152′[0.42]	135′[0.00]	− 23.09	1628	

[a]Fundamental vibrations, assigned as n^q, where n is the excited normal mode, and q its quantum number. These correspond to totally symmetric modes or vibronically induced nonsymmetric modes.
[b]Frequencies relative to the electronic origin band.
[c]Relative peak intensity, the 0-0 origin band intensity is 100.
[d]Dimensionless displacement.
[e]In square brackets the $J(m'_x, n)^2$, values = 0.00 are actually values <0.005.
[f]$\Delta\omega = \omega - \omega_{m'1}$.
[g]The values in Ar matrix published by VanCott *et al.*[28]
[h]The values in Ar matrix reported by Murray *et al.*[35]

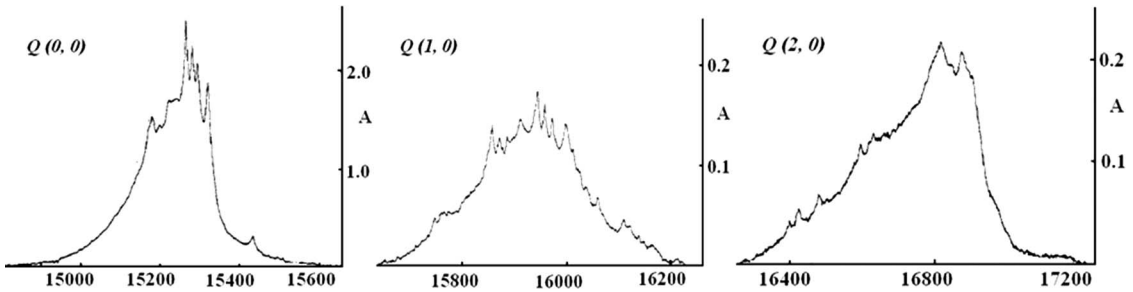

FIG. 4. Experimental absorption spectrum of ZnPc/Ar in the region of Q (0, 0), Q (1, 0), and Q (2, 0) envelopes, at ~5 K.

8 and 11, the mode with 311.91 cm^{-1} is from the combination of modes 12 and 21. Experimentally, they may be totally washed out by inhomogeneous broadening or coupling with the neighbor vibrational bands. The Q (1, 0) region could be well accounted for in terms of the vibronic bands in our simulation. We assigned the 45^1(506.86 cm^{-1}), 54^1(598.43 cm^{-1}), 64^1(686.23 cm^{-1}), 68^1(722.80 cm^{-1}), and 79^1(851.16 cm^{-1}) vibronic transitions as five fundamentals located at 479 (478), 589 (586), 676 (675), 739 (742), and 840 (851) cm^{-1} in experimental work.[28,35] The most intense vibrational band in this region located at 686.23 cm^{-1}, the relative intensity (9.8) is about one-tenth of the 0-0 transition. In the region of Q (2, 0), the existence of a positive B term in MCD indicates the additional presence of a separate electronic band, called Q' band which was suggested to arise from the z-polarized lowest $n \rightarrow \pi^*$ transition at 2.08 eV.[28,68] Mack and Stillman also assigned this band to the e_u (N_m lone pairs) $\rightarrow e_g$ (LUMO) transition centered at 2.05 eV.[32] For the D_{4h} symmetry of ZnPc, the four N_m lone pair combinations transform as e_u, b_{2g}, a_{1g} and the four N_p one pair combinations transform as e_u, b_{1g}, a_{1g}. From the percentage contribution of individual atoms to MOs of ZnPc (presented in the supplementary material[73]), we can determine the N_m related to the ZnPc orbitals are HOMO-9 (b_{2g}), HOMO-11/12 (e_u), and HOMO-14 (a_{1g}) with the orbital energies −7.24, −7.72, and −8.45 eV. The transitions interrelated with N_m lone pairs appear in the energy region of B band, which associated with the $\pi \rightarrow \pi^*$ transitions, such as the involved π orbitals HOMO-4 (a_{2u}), HOMO-10 (a_{2u}), and HOMO-13 (a_{1u}), their orbital energies are 7.02, 7.18, and 7.73 eV, respectively. So, the symmetry allowed $n \rightarrow \pi^*$ transitions are expected to contribute to the B band rather than the slightly blue side of the Q region. In our TD calculation of ZnPc absorption spectrum (presented in the supplementary material[73]), the lowest z-polarized state, the $1A_{2u}$, lies at 3.9117 eV, about 1.86 eV higher than experimental data. However, our calculated excitation energies are in accordance with previous published theoretical data.[33,37,59] It is noteworthy that the difference between the calculated data and experimental data is inevitable here despite the great efforts paid, but the credibility of our theoretical work should be above suspicion in a sense. Actually, from the separated HOMO (−5.17 eV) and HOMO-1 (−6.94 eV) orbitals, we also did not expect the $n \rightarrow \pi^*$ will appear in the region of Q band. Our simulated well-resolved spectrum profile is in agreement with the experimental result,[28] but we could not find any allowed excited state in the Q (2, 0) region. The conclusion also can be found in other works.[37,59] The intensity borrowing arose the activities of some weak modes would dominate the Q (2, 0) envelope. The mode 147 shows the maximal relative intensity and is stronger than mode 64 in Q (1, 0), which in accordance with experimental spectral profile.[28] Compared the FC and FCHT absorption spectra, one primarily difference was observed at the range of 1300–1500 cm^{-1}. One dominant congestion can be shaped along modes ν_{125}, ν_{126}, and ν_{140} in the FCHT spectrum, their frequencies are 1319.18, 1345.69, and 1491.39 cm^{-1}. Inspection of the data in Table III showed that the Duschinsky mixing is large for the three modes. Mode ν_{125} (1319.18 cm^{-1}) is mainly projected on three modes of ground state, ν_{120}' (1318.24 cm^{-1}), ν_{125}' (1343.02 cm^{-1}), and ν_{126}' (1343.02 cm^{-1}), the mixed modes with the values of Duschinsky matrix elements are $J[120', 125]^2 = 0.39$, $J[125', 125]^2 = 0.32$, and $J[126', 125]^2 = 0.24$, respectively. The mode ν_{126} mixed with ν_{125}' (1343.02 cm^{-1}), ν_{126}' (1343.02 cm^{-1}), and ν_{128}' (1362.15 cm^{-1}), the values of Duschinsky matrix elements are $J[126', 126]^2 = 0.45$, $J[125', 126]^2 = 0.35$, and $J[128', 126]^2 = 0.11$. Mode ν_{140} was projected on modes ν_{138}' (1491.87 cm^{-1}), ν_{144}' (1512.26 cm^{-1}), and ν_{145}' (1512.26 cm^{-1}), the mixed modes with the $J[120', 125]^2 = 0.39$, $J[125', 125]^2 = 0.32$, and $J[126', 125]^2 = 0.24$, respectively. Obviously, from Fig. 2 we can see that the Duschinsky effects make for the intensities redistribution of several vibronic bands. Such as the modes 76, 102, and 150 were nearly invisible in the HT' plot but prominent in HT plot, which indicated the corresponding intensities of those vibronic bands nearly come from the Duschinsky mixing.

The emission spectrum (presented in Fig. 3) was simulated and compared with the Shpol'skii data reported by Huang *et al.*[69] Recently, the splitting of the Q band absorption has been determined more accurately by Murray *et al.*[35] The emission spectra trapped in Ne, N_2, Ar, Xe, Kr matrices have been recorded in the region of the Q state. Comparison of emission and absorption spectra showed deviation from mirror symmetry that was more evident when looking to the assignments close to the 0-0 transition. The mirror symmetry breakdown close to the 0-0 transition originated from the frequency discrepancies of the modes involved in the spectra between ground state and excited state. Mode 7 located at 48.63 cm^{-1} in the S_1 state, the variation is 29 cm^{-1} compared with 7′ in S_0 state. Mode 8 located at 57.19 cm^{-1} in the S_1 state, the frequency of mode 8′ is 29.05 cm^{-1}, the

discrepancy was 28.14 cm^{-1}. So the vibrational bands involved modes 7 and 8 lied closer to the 0-0 transition in the fluorescence spectrum. The closest peak to 0-0 transition is located at 34 cm^{-1} in Ar matrix determined by Murray.[35] It is accordance with the 39.26 cm^{-1} in our simulated fluorescence spectrum. In addition to 0-0 transition, the highest peak is located at the Q (2, 0) region and originated from the excitation of mode 147 (1560.35 cm^{-1}) in absorption spectrum and 147′ (1561.33 cm^{-1}) in emission spectrum. The values of Duschinsky matrix elements corresponded to the mode 147 are $J[147', 147]^2 = 0.88$, $J[146', 147]^2 = 0.09$, and $J[134', 147]^2 = 0.01$ in absorption spectrum. The peak could be comparative with the experimental data of strong transition at 1565 cm^{-1}.[35] While the mode 147′ mainly projected on mode ν_{147} ($J[147', 147]^2 = 0.88$), ν_{146} ($J[146', 147]^2 = 0.08$), and ν_{135} ($J[135', 147]^2 = 0.01$) in the emission spectrum. The second highest one is located in the region of Q (1, 0), which derives from the excitation of mode 64 (686.23 cm^{-1}) in absorption. It fully projected on mode 63′. The second highest peak in fluorescence spectrum arises from the excitation of mode 63 (689.75 cm^{-1}). Our simulated peaks could be similar to the experimental results of the strong transition at 675 and 676 cm^{-1} in absorption spectrum,[28,35] 681 and 689 cm^{-1} in emission.[35,69] They are fully projected on each other with a weight of 1 ($J[63', 64]^2 = 1$ in absorption and $J[64', 63]^2 = 1$ in emission spectra), which indicated that these two normal modes are physically the same. In this way, compared the vibrational bands between fluorescence and absorption spectra would aid considerably in the identifications of the true vibrational bands.

2. The absorption and fluorescence spectra of ZnTBP

The FC and FCHT absorption spectra of ZnTBP were presented in Fig. 2, the 0-0 transition was found to carry most of the Franck-Condon intensity. The comparison of the FC and FCHT spectra profile showed the strong impact of the HT terms on the spectra. The simulated FCHT reproduced the experimental spectral profile well and in accord with the available data in Ar matrix and in supersonic expansions.[16,31,70,71] These spectra are in many ways typical of the metalloporphyrins and similar to those of ZnPc. We here carried out detailed analysis of FCHT spectra and assigned the involved vibrational modes with their relative intensities, as shown in Table IV. For convenience, the absorption spectrum will be discussed firstly. In the Gouterman's four-orbital model, the Q and *Soret* bands are ascribed to the admixture of the excitations HOMO (a_{1u}) → LUMO (e_g) and HOMO-1 (a_{2u}) → LUMO (e_g). The associated transition moments are taken to interfere destructively for the Q and constructively for the B transition. Therefore, the Q band ($f = 0.175$) is substantially weak and the B band is strong ($f = 1.136$) in absorption, as shown in Table II.

We divided the spectrum for three envelopes, Q' (0, 0), Q' (1, 0), and Q' (2, 0), according to the traditional labels of ZnPc. VanCott *et al.* investigated the Q band absorption and MCD spectra for ZnTBP.[31] Vibrational normal modes extended 1800 cm^{-1} to the blue side of the 0-0 origin band had been determined in their work. In the present work, the envelope of Q' (0, 0) was dominated by excitations of modes 7^2, 8^2, 20^1, 24^1,and 28^1, and their locations are 72.64, 125.50, 137.38, 221.89, and 244.35 cm^{-1} relative to the 0-0 origin

TABLE IV. Relevant normal modes of the electronic states in the FCHT fluorescence spectrum of ZnPc, calculated with B3LYP/def-TZVP.

State S_0				State S_1					
n[a]	ω[b]	i[c]	δ[d]	$m'1$[e]	$m'2$[e]	$m'3$[e]	$\Delta\omega$[f]	ω_{exp}[g]	ω_{exp}[h]
7^2	39.26	9.6	0.000	7′[0.98]	21′ [0.02]		− 29.00	34	
8^2	58.1	5.8	0.000	8′[0.96]	16′[0.03]	27′[0.00]	− 28.14		
11^2	124.3	1.8	0.000	11′[0.99]	24′[0.01]		− 23.18	102	125
20^1	158.20	2.5	0.226	20′[1.00]			0.93	161	
30^1	258.39	1.4	0.177	30′[1.00]			0.87	260	
54^1	601.39	2.3	0.230	54′[1.00]			2.96	598	592
63^1	689.75	8.1	− 0.435	64′[1.00]			3.52	689	681
68^1	728.76	4.0	0.000	62′[0.94]	76′[0.04]	74′[0.01]	5.96		
69^1	765.36	3.9	− 0.303	69′[1.00]			4.05	751	750
79^1	851.78	1.7	− 0.208	73′[1.00]			0.62	845	836
111^1	1165.70	3.0	− 0.272	112′[0.98]	116′[0.01]	115′[0.01]	− 3.05	1150	1143
125^1	1343.02	2.3	0.000	126′[0.35]	125′[0.32]	123′[0.18]	− 2.67	1346	1342
130^1	1372.09	2.5	− 0.254	130′[0.98]	120′[0.01]	147′[0.00]	− 12.96		
138^1	1491.87	4.2	0.000	140′[0.58]	137′[0.33]	139′[0.04]	0.48	1448	
147^1	1561.33	9.9	0.525	147′[0.88]	146′[0.08]	135′[0.01]	0.98	1525	1518
150^1	1617.44	1.3	0.000	149′[0.99]	140′[0.01]		10.47	1624	

[a]Fundamental vibrations, assigned as n^q, where n is the excited normal mode, and q its quantum number. These correspond to totally symmetric modes or vibronically induced nonsymmetric modes.
[b]Frequencies relative to the electronic origin band.
[c]Relative peak intensity, the 0-0 origin band intensity is 100.
[d]Dimensionless displacement.
[e]In square brackets the $J(m'_x, n)^2$, values = 0.00 are actually values <0.005.
[f]$\Delta\omega = \omega - \omega_{m'1}$.
[g]The values in Ar matrix published by Murra *et al.*[35]
[h]The Shpol'skii data reported by Huang *et al.*[69]

TABLE V. Relevant normal modes of the electronic states in the FCHT absorption spectrum of ZnTBP, calculated with B3LYP/def-TZVP.

State S_1				State S_0					
n[a]	ω[b]	i[c]	δ[d]	$m'1$[e]	$m'2$[e]	$m'3$[e]	$\Delta\omega$[f]	ω_{exp}[g]	ω_{exp}[h]
7^2	72.64	4.8	0.000	7′[0.99]	16′[0.01]		17.61		
8^2	125.50	1.8	0.000	8′[1.00]			16.90	129	123
20^1	137.38	3.3	0.000	20′[0.99]	16′[0.00]	29′[0.00]	4.38		
24^1	221.89	1.4	0.000	24′[0.92]	23′[0.08]		3.84		238
28^1	244.35	5.5	−0.325	28′[1.00]			−1.09	243	248
45^1	504.04	2.5	0.000	46′[1.00]			−0.95		515
55^1	594.71	1.0	−0.130	55′[1.00]			−3.07	583	577
66^1	677.02	2.9	0.000	66′[0.98]	63′[0.01]	73′[0.00]	−5.46		
68^1	707.62	5.3	−0.307	68′[1.00]			−3.22	691	691
69^1	748.11	3.2	0.232	72′[1.00]			−6.65		739
75^1	762.70	8.8	0.000	73′[0.80]	69′[0.19]	66′[0.00]	7.70		764
82^1	823.57	3.3	0.000	82′[1.00]			−9.34	824	820
83^1	845.31	3.0	0.231	83′[1.00]			0.46		845
101^1	1038.48	2.5	−0.041	100′[0.62]	103′[0.38]		−0.95	1023	1032
106^1	1068.97	4.3	0.000	105′[0.74]	106′[0.20]	109′[0.02]	−10.70		
111^1	1127.68	3.6	0.000	112′[0.52]	110′[0.40]	106′[0.03]	−17.30	1107	1121
122^1	1219.06	2.3	0.000	122′[0.86]	126′[0.07]	118′[0.04]	−2.19		
126^1	1286.50	1.8	0.000	126′[0.80]	128′[0.09]	122′[0.06]	19.32	1262	1274
131^1	1332.58	1.7	0.000	128′[0.83]	133′[0.10]	126′[0.05]	5.45	1316	1315
133^1	1355.65	6.1	−0.328	134′[0.75]	135′[0.22]	124′[0.01]	−6.08		1350
137^1	1402.86	3.1	0.000	137′[0.99]	133′[0.00]	128′[0.00]	−6.83	1379	1388
141^1	1443.33	3.2	0.000	141′[0.97]	150′[0.03]		−6.15	1450	1466
149^1	1507.63	9.2	0.000	149′[0.96]	153′[0.02]	145′[0.01]	−12.27	1515	1516
155^1	1599.95	6.4	0.149	155′[0.83]	158′[0.14]	163′[0.02]	−5.53		
161^1	1626.37	2.6	0.219	163′[0.83]	158′[0.09]	155′[0.08]	−24.54		

[a]Fundamental vibrations, assigned as n^q, where n is the excited normal mode, and q its quantum number. These correspond to totally symmetric modes or vibronically induced nonsymmetric modes.
[b]Frequencies relative to the electronic origin band.
[c]Relative peak intensity, the 0-0 origin band intensity is 100.
[d]Dimensionless displacement.
[e]In square brackets the $J(m'_x, n)^2$, values = 0.00 are actually values <0.005.
[f]$\Delta\omega = \omega - \omega_{m'1}$.
[g]The values in Ar matrix published by VanCott *et al.*[31]
[h]The values in supersonic expansion reported by Even *et al.*[71]

band (see Table V and Fig. 2). There are three fundamental vibrational excitations in energy range E = 0–400 cm^{-1} above the electronic origin of 0-0 band, which are located at 123, 238, and 248 cm^{-1} in supersonic expansion measurement.[71] The locations of the closest peak to the 0-0 origin band in experimental spectrum were reported at 123 cm^{-1} in supersonic expansion and 129 cm^{-1} in Ar matrix.[31,71] In the region of $Q'(1, 0)$, the spectrum is shaped by modes 45 (504.04 cm^{-1}), 55 (594.71 cm^{-1}), 66 (677.02 cm^{-1}), 68 (707.62 cm^{-1}), 69 (748.11 cm^{-1}), 75 (762.70 cm^{-1}), 82 (823.57 cm^{-1}), and 83 (845.31 cm^{-1}). Their relative intensities are 2.5, 1.0, 2.9, 5.3, 3.2, 8.8, 3.3, and 3.0. There were seven peaks appeared in this region with the associative experimental frequencies[71] 515, 577, 691, 739, 764, 820, and 845 cm^{-1}, indicating the excellent consistency between our theoretical results and the experimental observations. Our calculations showed that the Duschinsky mixing, mode 75 (the highest band in this region) with the frequency 762.70 cm^{-1}, is larger than other modes in $Q'(1, 0)$ region. It projected on the modes 73′(755.00 cm^{-1}), 69′(753.11 cm^{-1}), and 66′(682.48 cm^{-1}) with the $J[73', 75]^2 = 0.80$, $J[69', 75]^2 = 0.19$, and $J[66', 75]^2 = 0.00$ (values = 0.00 are actually values < 0.005). In the envelope $Q'(2, 0)$, modes 101, 106, 111, 122, 126, 131, 133, 137, 141, 149, 155, and 161 are assigned with the corresponding frequencies 1038.48, 1068.97, 1127.68, 1219.06, 1286.50, 1332.58, 1355.65, 1402.86, 1443.33, 1507.63, 1599.95, and 1626.37 cm^{-1}. Duschinsky mixing is obvious in this region, the maximal values of Duschinsky matrix in each mode are $J[100', 101]^2 = 0.62$, $J[105', 106]^2 = 0.74$, $J[112', 111]^2 = 0.52$, $J[122', 122]^2 = 0.86$, $J[126',126]^2 = 0.80$, $J[128', 131]^2 = 0.83$, $J[134', 133]^2 = 0.75$, $J[137', 137]^2 = 0.99$, $J[141', 141]^2 = 0.97$, $J[149', 149]^2 = 0.96$, $J[155', 155]^2 = 0.83$, and $J[163', 161]^2 = 0.83$, respectively. Compared the HT and *HT′* spectra in Fig. 2, we can also conclude that the Duschinsky contributions were important in the $Q'(2, 0)$ region. These vibronic bands with heavy Duschinsky mixing were labeled in the HT and *HT′* plots for comparison.

The emission spectrum of ZnTBP in *n*-octane single crystal was investigated by Fielding *et al.*,[70] the intensity of the strongest vibrational transition in fluorescence did not exceed one-thirtieth of the 0-0 origin band.[70] Similar result was observed in our simulation, and the most intense band (the relative intensity is 8.7, about one-twelfth of the 0-0 band) is from the excitation of mode 72 with frequency 754.76 cm^{-1}. The

TABLE VI. Relevant normal modes of the electronic states in the FCHT fluorescence spectrum of ZnTBP, calculated with B3LYP/def-TZVP.

State S_0				State S_1					
n[a]	ω[b]	i[c]	δ[d]	$m'1$[e]	$m'2$[e]	$m'3$[e]	$\Delta\omega$[f]	ω_{exp}[g]	ω_{exp}[h]
7^2	37.42	5.3	0.000	7′[0.99]	15′[0.01]		− 17.61	18	
9^2	85.08	3.1	0.000	9′[1.00]			− 28.52		
20^1	133.00	3.1	0.000	20′[0.99]	9′[0.00]	24′[0.00]	− 4.38	131	137
23^1	218.05	1.4	0.000	23′[0.92]	24′[0.08]		− 3.22		
28^1	245.44	4.9	0.324	28′[1.00]			1.09	242	244
45^1	504.99	2.3	0.000	45′[1.00]			− 1.82	482	486
66^1	682.48	3.1	0.000	66′[0.98]	62′[0.01]	75′[0.00]	5.46		
68^1	710.84	3.8	− 0.303	68′[1.00]			3.22	703	703
72^1	754.76	8.7	0.225	69′[1.00]			− 7.70	745	740
83^1	844.85	2.4	− 0.233	83′[1.00]			− 0.46	827	827
101^1	1039.85	1.2	0.000	101′[1.00]			1.42		
105^1	1079.67	2.0	0.000	106′[0.74]	107′[0.20]	113′[0.02]	10.70	1074	1066
112^1	1144.98	4.2	0.000	111′[0.52]	115′[0.46]	122′[0.01]	17.30	1160	1159
121^1	1221.25	3.9	0.000	123′[0.95]	125′[0.02]	119′[0.01]	− 4.33	1238	
125^1	1267.18	1.2	0.000	125′[0.88]	132′[0.05]	123′[0.03]	− 2.33	1251	1253
134^1	1361.73	3.0	0.278	133′[0.75]	134′[0.24]	124′[0.00]	6.08	1351	
137^1	1409.69	2.4	0.000	137′[0.99]	135′[0.01]		6.83		
140^1	1449.48	2.8	0.000	142′[0.93]	135′[0.03]	154′[0.02]	1.53	1457	1456
149^1	1519.90	7.1	0.000	149′[0.96]	154′[0.02]	147′[0.01]	12.27		
152^1	1582.53	1.0	0.000	153′[0.91]	160′[0.03]	158′[0.03]	11.16	1573	1570
157^1	1611.85	4.2	0.000	156′[0.96]	154′[0.02]	158′[0.01]	8.05	1626	1624
163^1	1650.91	2.8	− 0.273	161′[0.83]	157′[0.14]	155′[0.02]	24.54		

[a]Fundamental vibrations, assigned as n^q, where n is the excited normal mode, and q its quantum number. These correspond to totally symmetric modes or vibronically induced nonsymmetric modes.
[b]Frequencies relative to the electronic origin band.
[c]Relative peak intensity, the 0-0 origin band intensity is 100.
[d]Dimensionless displacement.
[e]In square brackets the $J(m'_x, n)^2$, values = 0.00 are actually values <0.005.
[f]$\Delta\omega = \omega - \omega_{m'1}$.
[g]The values in n-octane published by Fielding *et al.*[70]
[h]The values reported by Sevchenko *et al.*[72]

second highest peak located at 1519.90 cm^{-1} from the excitation of mode 149, the relative intensity is 7.1. Mode 72 fully projected on mode 69′ while mode 149 projected on three modes and mainly mixed with 149′, $J[149', 149]^2 = 0.96$. The high concentrations in $Q'(1, 0)$ and $Q'(2, 0)$ region are also consistent with those of Sevchenko *et al.* who analyzed the complex emission spectrum in a Shpol'skii matrix.[72] The collected data were presented in Table VI.

IV. CONCLUDING REMARKS

The absorption and emission spectra in the region of Q states of ZnPc and ZnTBP were simulated and fundamental vibrational assignments were carried out. In order to fully reproduce the rich vibrational structures and assign the vibronic modes of the $S_0 \leftrightarrow S_1$ optical spectra, it is necessary to account for the fact that the normal modes in an excited state generally could be not only distorted and displaced but also mixed with each other. In this work, the HT and Duschinsky mixing were considered separately, the pure HT (labeled *HT′*) and the summation of HT and Duschinsky contributions (labeled HT) were plotted for comparisons. For ZnPc, the redshift and intensification were discussed and analyzed with the calculation of vertical transition energies of low-lying excited states, the orbital energies, and the composition of the involved orbitals. We reaffirmed that the substitution of aza linkages for the methine bridges would lift the near degeneracy of the HOMO and HOMO-1. That reduces the configuration interaction of $a_{1u}{}^1e_g{}^1$ and $a_{2u}{}^1e_g{}^1$ and removes the forbidden character of electron transition, thus leads to the stronger Q band in phthalocyanine than in porphyrin. The absorption spectrum of ZnPc was divided into three major envelopes, traditionally labeled Q (0, 0), Q (1, 0), Q (2, 0). We assigned the weak vibrational transitions and compared those with experimental data reported by VanCott *et al.*[28] and Murray *et al.*[35] The similarity between our collected relative intensities, location sites, and the experimental results showed our simulations were reliable. Through the percentage contribution of individual atoms to molecular orbitals of ZnPc, we determined that the absence of electron transition ($n \rightarrow \pi^*$) in the Q (2, 0) region. Furthermore, the comparison of emission and absorption spectra were analyzed which aid considerably in our identifications of the true band assignments in the region of Q states. The deviation from mirror symmetry near the 0-0 origin band showed the frequency differences between the initial and final states, which reflected the fact that the normal modes in an excited state is distorted (having different frequencies). The simulated fluorescence spectrum also kept consistent with the high resolved spectra performed by Huang *et al.*[69] and Murray *et al.*[35] For ZnTBP, the FCHT spectra can fully reproduce the experimental spectral profiles while the FC spectra were seriously defective in reproducing the

experimental data. So the HT contributions should be considerable for ZnTBP.

To sum up, the Duschinsky and Herzberg-Teller contributions to the electronic transition dipole moments are essential to assign the weak vibrational transitions and reproduce the experimental spectral profile. The FCHT can provide a full and rich vibronic structure so that the simulations could be comparable with the experimental high resolved spectra. It should be emphasized that the theoretical calculation could reproduce the detail feature of spectroscopy by simulating the high-resolved spectroscopy, which could help to understand photophysical properties when accurate calculations are carried out in the analysis of the experimental results.

ACKNOWLEDGMENTS

We acknowledge generous financial support from Natural Science Foundation of China (20803059, 21173169) and Chongqing Municipal Natural Science Foundation (2009BB6002). C. Zhu would like to thank National Science Council of the Republic of China under Grant No. 97-2113-M-009-010-MY3 for support.

[1] G. T. Byrne, R. P. Linstead, and A. R. Lowe, J. Chem. Soc. **1934**, 1017.
[2] R. P. Linstead and J. M. Robertson, J. Chem. Soc. **1936**, 1736.
[3] R. P. Linstead and E. G. Noble, J. Chem. Soc. **1937**, 933.
[4] J. S. Anderson, E. F. Bradbrook, A. H. Cook, and R. P. Linstead, J. Chem. Soc. **1938**, 1151.
[5] P. A. Barrett, D. A. Frye, and R. P. Linstead, J. Chem. Soc. **1938**, 1157.
[6] P. A. Barrett, R. P. Linstead, F. G. Rundall, and G. A. P. Tuey, J. Chem. Soc. **1940**, 1079.
[7] *The Porphyrins*, edited by D. Dolphin (Academic, New York, 1978-1979).
[8] R. W. Wagner, J. S. Lindsey, J. Seth, V. Palaniappan, and D. F. Bocian, J. Am. Chem. Soc. **118**, 3996 (1996).
[9] J. R. Reimers, T.-X. Lu, M. J. Crossley, and N. S. Hush, Chem. Phys. Lett. **256**, 353 (1996).
[10] *Phthalocyanines: Properties and Applications*, edited by C. C. Leznoff and A. B. P. Lever (VCH, New York, 1990–1996), Vol. 1–4.
[11] A. Hagfeldt, G. Boschloo, L. C. Sun, L. Kloo, and H. Pettersson, Chem. Rev. **110**, 6595 (2010).
[12] S. Priyadarshy, M. J. Therien, and D. N. Beratan, J. Am. Chem. Soc. **118**, 1504 (1996).
[13] D. Beljonne, G. E. O'Keefe, P. J. Hamer, R. H. Friend, H. L. Anderson, and J. L. Brédas, J. Chem. Phys. **106**, 9439 (1997).
[14] O. Fenwick, J. K. Sprafke, J. Binas, D. V. Kondratuk, F. Di Stasio, H. L. Anderson, and F. Cacialli, Nano Lett. **11**, 2451 (2011).
[15] S. G. Bown, C. J. Tralau, P. D. Smith, D. Akdemir, and T. J. Wieman, Br. J. Cancer. **54**, 43 (1986).
[16] L. Bajema, M. Gouterman, and C. B. Rose, J. Mol. Spectrosc. **39**, 421 (1971).
[17] A. M. Schaffer, M. Gouterman, and E. R. Davidson, Theor. Chim. Acta **30**, 9 (1973).
[18] T.-H. Huang and J. H. Sharp, Chem. Phys. **65**, 205 (1982)
[19] T.-H. Huang, K. E. Rleckhoff, and E. M. Voigt, J. Phys. Chem. **85**, 3322 (1981).
[20] N. E. Khatib, B. Boudjema, and M. Maitro, Can. J. Chem. **66**, 2313 (1988).
[21] B. J. Prince, B. E. Williamsona, and R. J. Reeves, J. Lumin. **93**, 293 (2001).
[22] X. Liu, E. K. L. Yeow, S. Velate, and R. P. Steer, Phys. Chem. Chem. Phys. **8**, 1298 (2006).
[23] M. Gouterman, J. Chem. Phys. **30**, 1139 (1959).
[24] M. Gouterman, J. Mol. Spectrosc. **6**, 138 (1961).
[25] M. Gouterman, J. Mol. Spectrosc. **11**, 108 (1963).
[26] N. Kobayashi, T. Furuyama, and K. Satoh, J. Am. Chem. Soc. **133**, 19642 (2011).
[27] C. Weiss, H. Kobayashi, and M. Gouterman, J. Mol. Spectrosc. **16**, 415 (1965).
[28] T. C. VanCott, J. L. Rose, G. C. Misener, B. E. Williamson, A. Schrimpf, M. E. Boyle, and P. N. Schatz, J. Phys. Chem. **93**, 2999 (1989).
[29] D. H. Metcalf, T. C. VanCott, S. W. Snyder, and P. N. Schatz, J. Phys. Chem. **94**, 2828 (1990).
[30] B. E. Wilhuus, T. C. VanCott, J. L. Rose, A. Schrimpf, M. Koralewski, and P. N. Schatz, J. Phys. Chem. **95**, 6835 (1991).
[31] T. C. VanCott, M. Koralewski, D. H. Metcalf, and P. N. Schatz, J. Phys. Chem. **97**, 7417 (1993).
[32] J. Mack and M. J. Stillman, J. Phys. Chem. **99**, 7935 (1995).
[33] G. A. Peralta, M. Seth, H. Zhekova, and T. Ziegler, Inorg. Chem. **47**, 4185 (2008).
[34] C. Murray, N. Dozova, J. G. McCaffrey, S. FitzGerald, N. Shafizadeh, and C. Crépin, Phys. Chem. Chem. Phys. **12**, 10406 (2010).
[35] C. Murray, N. Dozova, J. G. McCaffrey, S. FitzGerald, N. Shafizadeh, W. Chin, and C. Crépin, Phys. Chem. Chem. Phys. **13**, 17543 (2011).
[36] E. J. Baerends, G. Ricciardi, A. Rosa, and S. J. A. van Gisbergen, Coord. Chem. Rev. **230**, 5 (2002).
[37] G. Ricciardi and A. Rosa, J. Phys. Chem. A. **105**, 5242 (2001).
[38] D. Sundholm, Chem. Phys. Lett. **302**, 480 (1999).
[39] A. Rosa, G. Ricciardi, E. J. Baerends, and S. J. A. van Gisbergen, *Eighth International Conference on the Applications of Density Functional Theory to Chemistry and Physics*, Rome, Italy, 1999.
[40] A. Rosa and G. Ricciardi, J. Phys. Chem. A. **105**, 3311 (2001).
[41] A. B. J. Parusel and S. Grimme, J. Porphyr. Phthalocyanines **5**, 225 (2001).
[42] M. Dierksen and S. Grimme, J. Chem. Phys. **120**, 3544 (2004).
[43] J.-L. Chang, J. Chem. Phys. **128**, 174111 (2008).
[44] K. A. Nguyen and R. Pachter, J. Chem. Phys. **118**, 5802 (2003).
[45] A. M. Mebel, M. Hayashi, K.-K. Liang, and S.-H. Lin, J. Phys. Chem. A **103**, 10674 (1999).
[46] M. Dierksen and S. Grimme, J. Phys. Chem. A **108**, 10225 (2004).
[47] S. Grimme, Rev. Comput. Chem. **20**, 153 (2004).
[48] M. Dierksen and S. Grimme, J. Chem. Phys. **122**, 244101 (2005).
[49] F. Santoro, R. Improta, A. Lami, J. Bloino, and V. Barone, J. Chem. Phys. **126**, 084509/1 (2007).
[50] F. Santoro, R. Improta, A. Lami, J. Bloino, and V. Barone, J. Chem. Phys. **126**, 184102 (2007).
[51] F. Santoro, A. Lami, R. Improta, J. Bloino, and V. Barone, J. Chem. Phys. **128**, 224311/1 (2008).
[52] L. S. Cederbaum and W. Domcke, J. Chem. Phys. **64**, 603 (1976).
[53] J. Guthmuller and B. Champagne, J. Chem. Phys. **127**, 164507/1 (2007).
[54] M. Parac and S. Grimme, Chem. Phys. **292**, 11 (2003).
[55] R. Ahlrichs, M. Bär, and H. P. Baron, *et al.* TURBOMOLE, version 6.2, University of Karlsruhe, 2010.
[56] F. Duschinsky, Acta Physicochim. URSS **7**, 551 (1937).
[57] G. Herzberg and E. Teller, Z. Phys. Chem. Abt. B **21**, 410 (1933).
[58] F. Santoro, FCclasses, a Fortran 77 code, see http://village.ipcf.cnr.it.
[59] K. A. Nguyen and R. Pachter, J. Chem. Phys. **114**, 10757 (2001).
[60] W. R. Scheidt and W. Dow, J. Am. Chem. Soc. **99**, 1101 (1977).
[61] L. K. Lee, N. H. Sabelll, and P. R. LeBreton, J. Phys. Chem. **86**, 3926 (1982).
[62] A. J. McHugh, M. Gouterman, and C. Weiss, Theor. Chim. Acta **24**, 346 (1972).
[63] F. L. Plows and A. C. Jones, J. Mol. Spectrosc. **194**, 163 (1999).
[64] R. P. Linstead and F. T. Weiss, J. Chem. Soc. 2975 (1950).
[65] L. Edwards, M. Gouterman, and C. B. Rose, J. Am. Chem. Soc. **98**, 7638 (1976).
[66] U. Even and J. Jortner, J. Phys. Chem. **86**, 2273 (1982).
[67] B. Minaev, Y.-H. Wang, G.-K. Wang, Y. Luo, and H. Ågren, Spectrochim. Acta, Part A **65**, 308 (2006).
[68] G. J. Small, J. Chem. Phys. **54**, 3300 (1971).
[69] T.-H. Huang, K. E. Rleckhoff, and E. M. Voigt, J. Chem. Phys. **77**, 3424 (1982).
[70] P. E. Fielding and A.W.-H. Mau, Aust. J. Chem. **29**, 933 (1976).
[71] U. Even, J. Magen, J. Jortner, and J. Friedman, J. Chem. Phys. **77**, 4384 (1982).
[72] A. T. Gradyushko, A. N. Sevchenko, K. N. Solov'ev, and S. F. Shkirman, Sov. Phys. Dokl. **11**, 587 (1967).
[73] See supplementary material at http://dx.doi.org/10.1063/1.3703310 for calculated energies of frontier molecular orbitals, percentage contribution of individual atoms to molecular orbitals, calculated vertical transition energies, and oscillator strengths of e_u (N_m lone pairs) $\rightarrow e_g$, all frequencies of ground and excited states, and simulated spectrum with FWHM of 0.05 eV and experimental spectrum of ZnPc, and so on.